MASS DEFICITS, STALLING RADII, AND THE MERGER HISTORIES OF ELLIPTICAL GALAXIES

DAVID MERRITT

Department of Physics, Rochester Institute of Technology, Rochester, NY 14623
Draft version February 5, 2008

Abstract

A binary supermassive black hole leaves an imprint on a galactic nucleus in the form of a "mass deficit," a decrease in the mass of the nucleus due to ejection of stars by the binary. The magnitude of the mass deficit is in principle related to the galaxy's merger history, but the relation has never been quantified. Here, high-accuracy N-body simulations are used to calibrate this relation. Mass deficits are shown to be $M_{def} \approx 0.5 M_{12}$, with M_{12} the total mass of the binary; the coefficient in this relation depends only weakly on M_2/M_1 or on the galaxy's pre-existing density profile. Hence, after $\mathcal{N}$ mergers, $M_{def} \approx 0.5 \mathcal{N} M_\bullet$ with $M_\bullet$ the final (current) black hole mass. When compared with observed mass deficits, this result implies $1 \lesssim \mathcal{N} \lesssim 3$, in accord with hierarchical galaxy formation models. Implications for binary stalling radii, the origin of hyper-velocity stars, and the distribution of dark matter at the centers of galaxies are discussed.

Subject headings:

1. INTRODUCTION

Galaxy mergers bring supermassive black holes (SBHs) together (Begelman, Blandford, & Rees 1980), and binary SBHs are increasingly invoked to explain the properties of normal and active galaxies (Komossa 2003), including AGN variability (Valtaoja et al. 2000; Xie 2003), the bending and precession of radio jets (Roos et al. 1993; Romero et al. 2000), X- and Z-shaped radio lobes (Merritt & Ekers 2002; Gopal-Krishna et al. 2003) and the presence of cores in bright elliptical galaxies (Milosavljevic et al. 2002; Graham 2004). Binary SBHs may also be responsible for the high-velocity stars observed in the halo of the Milky Way (Yu & Tremaine 2003; Haardt et al. 2006), and for other populations that appear to have been ejected from galaxies, including intra-cluster planetary nebulae (Holley-Bockelmann et al. 2005).

The dynamical interaction of a massive binary with stars in a galactic nucleus is often discussed with reference to rate equations derived from scattering experiments (Hills 1983; Mikkola & Valtonen 1992; Quinlan 1996). A massive binary hardens at a rate

$$\frac{d}{dt}\left(\frac{1}{a}\right) = H\frac{G\rho}{\sigma} \tag{1}$$

where a is the binary semi-major axis, ρ and σ are the stellar density and velocity dispersion, and H is a dimensionless rate coefficient that depends on the binary mass ratio, eccentricity, and hardness. The mass in stars ejected by the binary satisfies

$$\frac{dM_{ej}}{d\ln(1/a)} = JM_{12}, \tag{2}$$

where $M_{12} \equiv M_1 + M_2$, the binary mass, and J is a second dimensionless coefficient. Equations (1) and (2) have been used to estimate evolution rates of binary SBHs in galactic nuclei (e.g. Volonteri et al. 2003a, b; Sesana et al. 2004) and to compute the mass in stars ejected from the galaxy by the binary (e.g. Holey-Bockelmann et al. 2005; Haardt et al. 2006). These equations are also the basis for many hybrid schemes which imbed a binary into a model of the host galaxy (Zier & Biermann 2001; Yu 2002; Merritt & Wang 2005).

Equations (1) and (2) are not particularly useful however when computing the binary-induced change in the distribution of stars in a nucleus, which is the topic of the current paper. N-body experiments show that the two SBHs substantially change the stellar density in a short time, of order the galaxy crossing time or less, *before* they form a tightly-bound pair (e.g. Figure 4 of Milosavljevic & Merritt 2001). In other words, by the time that equations like (1) and (2) start to become valid, a considerable change has already taken place in the stellar distribution. Furthermore, in many galaxies, evolution of the binary would be expected to stall at about the same time that it becomes hard (Valtonen 1996). Even if the mass ejected by the binary before this time could be accurately computed from an equation like (2), it would still be difficult to relate M_{ej} to observable changes in the nuclear density profile.

N-body techniques would seem to be the solution to these problems; but N-body integrations are plagued by spurious relaxation and other discreteness effects, which cause an embedded binary to continue evolving even in circumstances where a real binary would stall (Berczik, Merritt & Spurzem 2005). The counterpart of these discreteness effects in real galaxies is two-body relaxation, but – especially in the luminous galaxies that show evidence of the "scouring" effects of a massive binary – central relaxation times are much too long to significantly affect the supply of stars to the binary (Yu 2002). N-body simulations that are dominated by discreteness effects can not be scaled to the essentially collisionless regime of real galaxies.

However, there has been much progress in the art of N-body simulation in recent years, such that high-accuracy, direct-summation integrations are now feasible with particle numbers as large as 10^6 (Dorband et al. 2003; Gualandris et al. 2004; Fukushige et al. 2005; Berczik, Merritt & Spurzem 2005). Given such high values of N, it becomes possible to separate the rapid, early phases of binary evolution – which, when appropriately normalized, should be independent of N – from the late, slow stages that are driven by N-dependent process like collisional loss-cone repopulation.

This is the approach adopted in the present paper. N-body simulations are used to follow the evolution of a galaxy containing a central massive object and a second, inspiralling point mass. The integrations are continued until the two massive particles form a tight binary. The time at which the evolution of the binary switches from rapid – i.e. N-independent

– to slow – i.e. N-dependent – is identified, and the properties of the galaxy are recorded at that time. The degree to which a clear separation of the two regimes is possible, for a given N, depends on the binary mass ratio, becoming more difficult as the mass ratio becomes more extreme. Results are presented here for mass ratios in the range $0.025 \leq M_2/M_1 \leq 0.5$.

We find (§4) that the *mass deficit* – the difference in integrated mass between initial and final nuclear density profiles – at the end of the rapid evolutionary phase is proportional to the total mass of the binary, $M_{def} \approx 0.5 M_{12}$, with only a weak dependence on M_2/M_1 or on the initial density profile. This result can be motivated by simple arguments (§2): the smaller M_2, the tighter the binary which it forms before stalling.

A mass deficit of $\sim 0.5 M_\bullet$ is at least a factor two smaller than the typical mass deficits observed in bright elliptical galaxies (Milosavljevic et al. 2002; Graham 2004; Ferrarese et al. 2006) but we show via an additional set of N-body simulations (§5) that the effect of binary SBHs on a nucleus is *cumulative*, scaling roughly in proportion both to the number of mergers and to the final mass of the SBH. Hence, observed values of $M_{def}/M_\bullet$ can be used to constrain the number $\mathcal{N}$ of mergers that have taken place since the era at which the SBHs first formed. We find (§6) that $1 \lesssim \mathcal{N} \lesssim 3$, consistent with expectations from hierarchical structure formation theory. Finally, in §7 and §8, the implications for binary stalling radii, ejection of high-velocity stars, and the distribution of dark matter are discussed.

2. STAGES OF BINARY EVOLUTION

Here we review the stages of binary SBH evolution and discuss the connection between evolution of a binary in N-body simulations and in real galaxies.

Let M_1 and M_2 to be the masses of the two components of the binary, and write $M_{12} \equiv M_1 + M_2$, $q \equiv M_2/M_1 \leq 1$, and $\mu \equiv M_1 M_2/M_{12}$. In what follows we assume that the larger SBH is located initially at the center of the galaxy and that the smaller SBH spirals in.

The evolution of the massive binary is customarily divided into three phases.

1. At early times, the orbit of the smaller SBH decays due to dynamical friction from the stars. This phase ends when the separation R_{12} between the two SBHs is $\sim r_h$, the gravitational influence radius of the larger hole. We define r_h in the usual way as the radius of a sphere around M_1 that encloses a stellar mass of $2M_1$:

$$M_\star(r_h) = 2M_1. \qquad (3)$$

2. When R_{12} falls below $\sim r_h$, the two SBHs form a bound pair. The separation between the two SBHs drops rapidly in this phase, due both to dynamical friction acting on M_2, and later to ejection of stars by the binary (Milosavljevic & Merritt 2001). The motion of the smaller SBH around the larger is approximately Keplerian in this phase; we denote the semi-major axis by a and the eccentricity by e. The relative velocity of the two SBHs for $e = 0$ is

$$V_{bin} = \sqrt{\frac{GM_{12}}{a}} \qquad (4)$$

and the binary's energy is

$$E = -\frac{GM_1 M_2}{2a}. \qquad (5)$$

3. The rapid phase of binary evolution comes to an end when the binary's binding energy reaches $\sim M_{12}\sigma^2$, i.e. when $a \approx a_h$, where a_h is the semi-major axis of a "hard" binary, sometimes defined as

$$a_h = \frac{G\mu}{4\sigma^2}. \qquad (6)$$

If one writes $r_h = GM_1/\sigma^2$ – equivalent to the definition (3) in a nucleus with $\rho \sim r^{-2}$ – then a_h can also be written

$$a_h = \frac{q}{(1+q)^2}\frac{r_h}{4}. \qquad (7)$$

The exact definition of a "hard" binary varies from author to author, and this vagueness reflects the difficulty of relating the evolution of an isolated binary to one embedded in a galaxy. An isolated binary in a fixed background begins to harden at an approximately constant rate, $(d/dt)(1/a) \approx$ const., when $a \lesssim a_h$ (Quinlan 1996). But in a real galaxy, a hard binary would efficiently eject all stars on intersecting orbits, and its hardening rate would suddenly *drop* at $a \approx a_h$. This effect has been observed in N-body experiments with sufficiently large N (Makino & Funato 2004; Berczik, Merritt & Spurzem 2005).

Supposing that the binary "stalls" at $a \approx a_h$, it will have given up an energy

$$\Delta E \approx -\frac{GM_1 M_2}{2r_h} + \frac{GM_1 M_2}{2a_h} \qquad (8a)$$

$$\approx -\frac{1}{2}M_2\sigma^2 + 2M_{12}\sigma^2 \qquad (8b)$$

$$\approx 2M_{12}\sigma^2 \qquad (8c)$$

to the stars in the nucleus. In other words, the energy transferred from the binary to the stars is roughly proportional to the *combined* mass of the two SBHs. This result suggests that the binary will displace a mass in stars of order its own mass, independent of the mass of the infalling hole. This prediction is verified in the N-body simulations presented below.

Since the "hard" binary separation a_h is ill-defined for binaries embedded in galaxies, we define here a more useful quantity. The *stalling radius* a_{stall} is defined as the separation at which evolution of the binary would halt, $d(1/a)/dt = 0$, in the absence of any mechanism to re-supply the stellar orbits. For instance, if the galaxy potential were completely smooth, the binary's decay would halt once all the stars on orbits intersecting the binary had been ejected or otherwise (e.g. due to shrinkage of the binary) stopped interacting with it. The motivation for this definition is the very long time scales, in luminous elliptical galaxies, for orbital re-population by two-body encounters. Even in galaxies with relatively short central relaxation times, the binary's hardening rate would drop drastically at $a = a_{stall}$ and the likelihood of finding the binary at a separation near a_{stall} would be high.

This definition implies a dependence of a_{stall} on the mass ratio of the binary, but (unlike Equation 6) it also implies a dependence on the initial density profile and shape (spherical, axisymmetric, triaxial) of the galaxy, since these factors may influence the mass in stars that can interact with the binary. The definition is operational: it can only be applied by "doing the experiment," i.e. imbedding the binary in a galaxy model, turning off gravitational perturbations (aside from those due to the binary itself), and observing when the decay halts.

In a numerical simulation with finite N, gravitational encounters will continue supplying stars to the binary at rates much higher than those in real galaxies. One can still estimate a_{stall} if the particle number is large enough that a clear

TABLE 1
PARAMETERS OF THE N-BODY INTEGRATIONS

γ	M_2/M_1	r_h	r_h'	$a_{\rm stall}$	$a_{\rm stall}/r_h'$	$M_{\rm def}/M_{12}$
0.5	0.5	0.264	0.37	1.49×10^{-2}	4.08×10^{-2}	0.60
0.5	0.25	0.264	0.32	1.18×10^{-2}	3.69×10^{-2}	0.46
0.5	0.1	0.264	0.30	5.38×10^{-3}	1.82×10^{-2}	0.33
0.5	0.05	0.264	0.29	3.60×10^{-3}	1.26×10^{-2}	0.27
0.5	0.025	0.264	0.28	1.91×10^{-3}	6.82×10^{-3}	0.24
1.0	0.5	0.165	0.24	7.75×10^{-3}	3.23×10^{-2}	0.62
1.0	0.25	0.165	0.22	4.83×10^{-3}	2.25×10^{-2}	0.54
1.0	0.1	0.165	0.19	2.37×10^{-3}	1.23×10^{-2}	0.45
1.0	0.05	0.165	0.19	1.36×10^{-3}	7.27×10^{-3}	0.39
1.0	0.025	0.165	0.18	6.21×10^{-4}	3.36×10^{-3}	0.34
1.5	0.5	0.0795	0.13	3.66×10^{-3}	2.77×10^{-2}	0.63
1.5	0.25	0.0795	0.11	2.18×10^{-3}	1.95×10^{-2}	0.56
1.5	0.1	0.0795	0.10	1.26×10^{-3}	1.29×10^{-2}	0.41
1.5	0.05	0.0795	0.10	7.78×10^{-4}	8.19×10^{-3}	0.38
1.5	0.025	0.0795	0.09	4.60×10^{-4}	4.84×10^{-3}	0.39

change takes place in the hardening rate at some value of a. Better still, by repeating the experiment with different values of N, one can hope to show that the rapid evolutionary phase comes to an end at a well-defined time and that subsequent evolution occurs at a rate that is a decreasing function of N.

One advantage of defining a_{stall} in this operational way is that it eliminates the need for many of the qualitative distinctions that have been made in the past between the different regimes of binary evolution, e.g. "soft binaries" vs. "hard binaries," hardening via "dynamical friction" vs. hardening via "loss-cone draining," etc. (Yu 2002). It also allows for mechanisms that are not reproduced in the scattering experiments on which Equations (1) and (2) are based, e.g. the "secondary slingshot" (Milosavljevic & Merritt 2003), or the effect of the changing nuclear density on the rate of supply of stars to the binary.

It would seem natural to compute a_{stall} using so-called "collisionless" N-body codes that approximate the gravitational potential via smooth basis functions (Clutton-Brock 1973; van Albada & van Gorkom 1977; Hernquist & Ostriker 1992). Such algorithms have in fact been applied to the binary SBH problem (Quinlan & Hernquist 1997; Hemsendorf et al. 2002; Chatterjee et al. 2003) but with results that are not always consistent with those of direct-summation codes or with the predictions of loss-cone theory (compare Chatterjee, Henquist & Loeb 2003 with Berczik, Merritt & Spurzem 2005). These inconsistencies may be due to difficulties associated with incorporating a binary into a collisionless code, ambiguities about the best choice of origin for the potential expansion, etc. Until these issues can be resolved, direct-summation N-body codes seem a safer choice.

3. MODELS AND METHODS

The galaxy models and N-body techniques used here are similar to those described in Merritt & Szell (2005) (hereafter Paper I). In brief, Monte-Carlo realizations of steady-state, spherical galaxy models were constructed using Dehnen's (1993) density law. The models contained an additional, central point mass representing the more massive of the two SBHs. The mass of this particle, M_1, was always set to 0.01 in units where the total mass in stars M_{gal} was one. (The Dehnen scale length r_D and the gravitational constant G are also set to unity in what follows.) Stellar positions and velocities were

generated from the unique isotropic phase-space distribution function that reproduces Dehnen's $\rho(r)$ in the combined gravitational potential of the stars and the central point mass. The second SBH was introduced into this model at $t = 0$, and given a velocity roughly $1/2$ of the circular orbital velocity. In the models with $\gamma = 0.5$ and $\gamma = 1.0$, the initial separation of the two massive particles was 1.6, while in the models with $\gamma = 1.5$ the initial separation was 0.5. Each realization was then integrated forward using the N-body integrator described in Merritt, Mikkola & Szell (2005), an adaptation of NBODY1 Aarseth (1999) to the GRAPE-6 special-purpose computer. Close encounters between the two SBH particles, and between the SBHs and stars, were regularized using the algorithm of Mikkola and Aarseth (Mikkola & Aarseth 1990, 1993).

Three parameters suffice to define the initial models: the binary mass ratio q, the central density slope of the Dehnen model $\gamma \equiv -d \log \rho / d \log r$, and the number of particles N. Five values of the binary mass ratio were considered: $q = (0.5, 0.25, 0.1, 0.05, 0.025)$. For each choice of q, three values of γ were used: 0.5, 1.0, and 1.5. Finally, each of these 15 initial models was integrated with two different values of N: 1.2×10^5 and 2.0×10^5. Mass deficits were computed as described in Paper I.

The parameters of the N-body integrations are summarized in Table 1. Columns three and four give two different estimates of the binary's influence radius. The first, r_h, is the radius containing a mass in stars equal to twice M_1 in the initial model. The second is the radius containing a mass in stars equal to twice $M_1 + M_2$ at a time $t = t_{stall}$, the estimated stalling time. The second definition, r_h', is the relevant one when comparing the results of the N-body integrations to a real galaxy which has already experienced the scouring effects of a binary SBH. The other columns in Table 1 give estimates of the stalling radius $a_{stall} \equiv a(t_{stall})$ and the mass deficit $M_{def}(t_{stall})$, derived as described below.

4. RESULTS

Figure 1 illustrates the evolution of the relative orbit in the five integrations with $\gamma = 1.5$ and $N = 200K$. The three phases discussed above are evident. (1) The separation R_{12} between the two massive particles gradually decreases as dynamical friction extracts angular momentum from the orbit of M_2. (2) When $R_{12} \approx r_h$, the rapid phase of binary evolution begins. (3) When the separation drops to $\sim a_h$, evolution again slows. Figure 1 shows clearly that the separation of the two massive particles at the start of the final phase is smaller for smaller M_2.

Figure 1 suggests that the stalling radius is of order a_h, but better estimates of a_{stall} can be made by comparing integrations of the same model carried out with different N. Figure 2 makes the comparison for the model with $\gamma = 1.0$ and $q = 0.1$. After ~ 15 orbits, the mean separation between the two massive particles has dropped from ~ 1 to $\sim 0.2 \approx r_h$ and the second, rapid phase of binary hardening begins. Prior to this time, the two integrations with different N find essentially identical evolution of R_{12}. As discussed above, the evolution during this phase is due to some combination of dynamical friction acting on M_2 and ejection of stars by the increasingly-hard binary, both of which are N-independent processes. The contribution of dynamical friction to the evolution can be estimated using Chandrasekhar's (1943) expression for the dy-
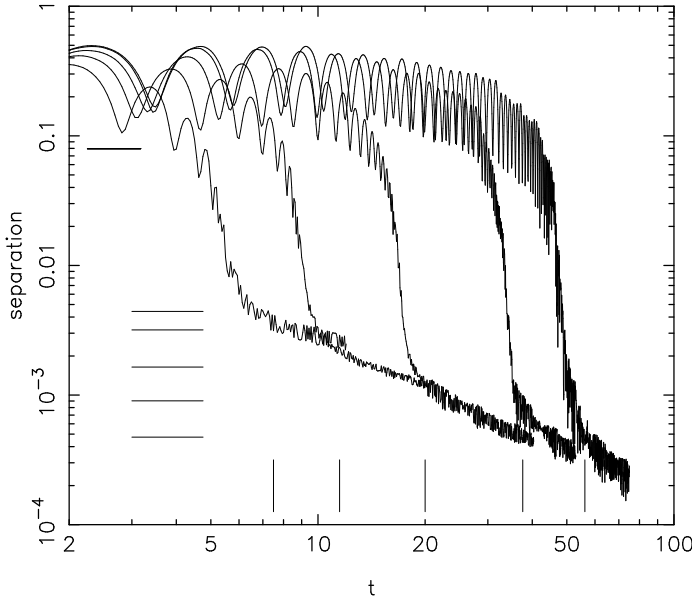
FIG. 1.— Evolution of the binary separation in five N-body integrations with $\gamma = 1.5$ and $N = 200$K; binary mass ratios are, from left to right, $0.5, 0.25, 0.1, 0.05, 0.025$. Vertical lines show the times identified as $t = t_{stall}$. The upper horizontal line indicates r_h, the influence radius of the more massive hole in the initial model. Lower horizontal lines show a_h as defined in Equation (7). The rapid phase of decay continues until $a \approx a_h$, with the result that the binary's binding energy at the end of this phase is nearly independent of M_2.

namical friction force:

$$\langle \Delta v_{\parallel} \rangle = -4\pi (4\pi G^2 M_2 \rho) \int_0^{\infty} dv_f \left(\frac{v_f}{v} \right)^2 f_f(v_f) H_1(v, v_f) \quad (9a)$$

$$H_1 = \begin{cases} \ln \Lambda \text{ if } v > v_f, \\ 0 \quad \text{if } v < v_f. \end{cases} \quad (9b)$$

This is the standard approximation in which $\ln \Lambda$ is "taken out of the integral"; v is the velocity of the massive object, v_f is the velocity of a field star, and $f_f(v_f)$ is the field-star velocity distribution, normalized to unit total number and assumed fixed in time. The result of integrating equation (9), with $\ln \Lambda = 5.7$, is shown in the upper panel of Figure 2 as the red (thin) line. Chandrasekhar's formula accurately reproduces the evolution of the relative orbit until a time $t \approx 80$, after which it predicts that the separation should drop to zero at a finite time. However as shown in the lower panel of Figure 2, by $t = 80$ – roughly at the start of the second evolutionary phase – the infall of M_2 has begun to displace stars and lower the central density, and the dynamical friction force must drop below the value predicted by equation (9) with fixed ρ and f_f.

The inset in Figure 2 shows the inverse semi-major axis of the binary, $1/a$, versus time in the two integrations of this model with different N. The two curves are coincident until $a \approx a_h$ but diverge at later times. This is the expected result (Berczik, Merritt & Spurzem 2005): once the hard binary has ejected most of the stars on intersecting orbits, continued hardening requires orbital repopulation which occurs on a time scale that is roughly proportional to N. The difference between the two integrations is also apparent in the lower panel of Figure 2, which shows mass deficits in the two integrations. Based on this comparison, the stalling radius – the value of a at which the evolution ceases to be independent of particle number – is $a_{stall} = a(t \approx 110) \approx 2 \times 10^{-3}$, and the mass deficit when $a = a_{stall}$ is $M_{def} \approx 0.5 M_1$.
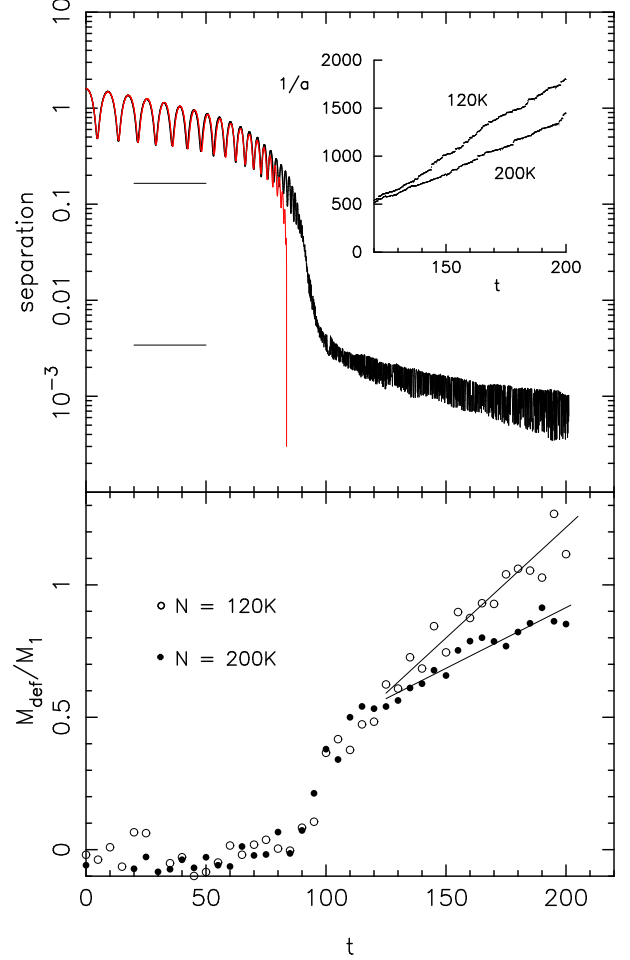

FIG. 2.— *Upper panel:* Thick (black) line shows evolution of the binary separation in the N-body integration with $\gamma = 1.0$, $M_2/M_1 = 0.1$, $N = 200$K. Thin (red) line is the evolution predicted by the dynamical friction equation (9) assuming a fixed galaxy. Horizontal lines indicate r_h and a_h, the latter as defined in Equation (7). The inset shows the evolution of the inverse semi-major axis of the binary for this integration, and for a second integration with $N = 120$K. *Lower panel:* The mass deficit, as defined in the text, for the same two N-body integrations. Lines show least-squares fits to the time intervals $80 \leq t \leq 110$ and $110 \leq t \leq 200$.

In order to make still more accurate estimates of t_{stall} and a_{stall}, the hardening rate,

$$s(t) \equiv \frac{d}{dt} \left(\frac{1}{a} \right), \quad (10)$$

was estimated from the N-body data by fitting smoothing splines to the measured values of a^{-1} vs. t and differentiating. In a collisionless galaxy, $s(t)$ would reach a peak value during the rapid phase of binary evolution, then drop rapidly to zero as the stars on intersecting orbits are ejected by the binary; t_{stall} would be the time at which $s \approx 0$. In the N-body integrations, s will never fall completely to zero since gravitational encounters continue to scatter stars into the binary's loss cone.

Figure 3 shows $s(t)$ as extracted from the N-body integrations with $\gamma = 0.5$. In each case, s reaches a peak value during the rapid phase of evolution and then declines. In the models with largest M_2, loss-cone repopulation is least efficient, and the hardening rates in the two integrations with different N "track" each other well past the peak. As M_2 is decreased, loss cone repopulation becomes more efficient and the two $s(t)$ curves deviate from each other at progressively earlier times with respect to the peak.
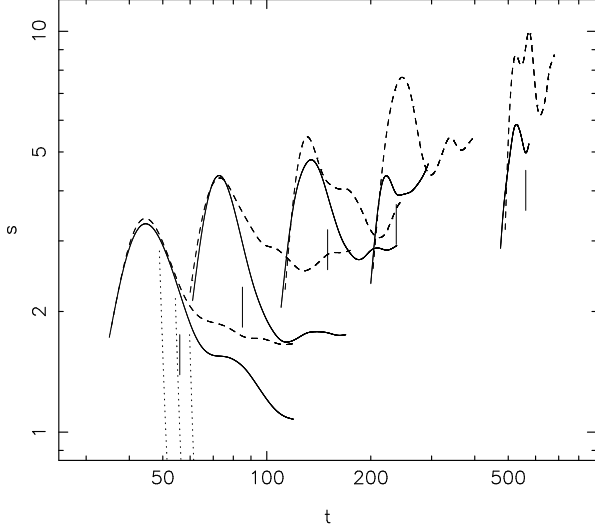
FIG. 3.— Evolution of the binary hardening rate $s \equiv (d/dt)(1/a)$ in N-body integrations with $\gamma = 0.5$; binary mass ratios are, from left to right, $0.5, 0.25, 0.1, 0.05, 0.025$. Solid curves are for $N = 200K$ and dashed curves are for $N = 120K$. Vertical solid lines are the estimates of t_{stall}. Nearly-vertical dashed lines show the approximate, asymptotic behavior of $s(t)$ in a purely collisionless galaxy, assuming $t(a_h) = (40, 50, 60)$.

Even in the absence of loss cone repopulation, a binary in a collisionless galaxy would continue to evolve at late times as stars with progressively longer orbital periods reach pericenter and interact with it. The asymptotic behavior of $s(t)$ in a spherical non-evolving galaxy in the absence of encounters is roughly

$$s(t) = \frac{d}{dt}\left(\frac{1}{a}\right) \approx 16\pi^2 K \int f_m(E) dE \qquad (11)$$

where $f_m(E)$ is the phase-space mass density of stars and K is a constant that defines the mean, dimensionless change of energy of the binary in one interaction with a star (Yu 2002). Equation (11) equates the rate of change of the binary's energy with the rate at which stars, moving along their unperturbed orbits, enter the binary's influence sphere and extract energy from it. Depopulation of the orbits as stars are ejected is represented by progressively restricting the range of the energy integral; the lowest allowed energy at any time t is that corresponding to an orbit with radial period $P(E) = t$. Following Yu (2002), we set $K = 1.6$, the approximate value for a "hard" binary, and assume that the integration starts at $a = a_h$. Figure 3 compares the solution to Equation (11) with the N-body hardening rates for $(\gamma = 0.5, q = 0.5)$. Clearly, the "draining" of long-period orbits contributes only minimally to the late evolution seen in the N-body integrations, i.e. the evolution in phase three is driven almost entirely by loss-cone repopulation.

Plots like those in Figure 3 were used to estimate t_{stall} for each $(\gamma, M_2/M_1)$. Unavoidably, these estimates are somewhat subjective. For the larger values of M_2, t_{stall} was taken to be the time when the $s(t)$ curves for the two different N-values begin to separate. For the integrations with smaller M_2, collisional effects are more important, and the two $s(t)$ curves separate even before the peak value is reached. In these integrations, t_{stall} was taken to be the time at which $s(t)$ in the $N = 200K$ integration reached its first minimum after the peak. These estimated t_{stall} values are likely to be systematically larger than the true values in a collisionless galaxy. However the uncertainties in the estimated values of $a_{stall} \equiv a(t_{stall})$ and $M_{def}(t_{stall})$ are probably modest, at least for the larger M_2 val-
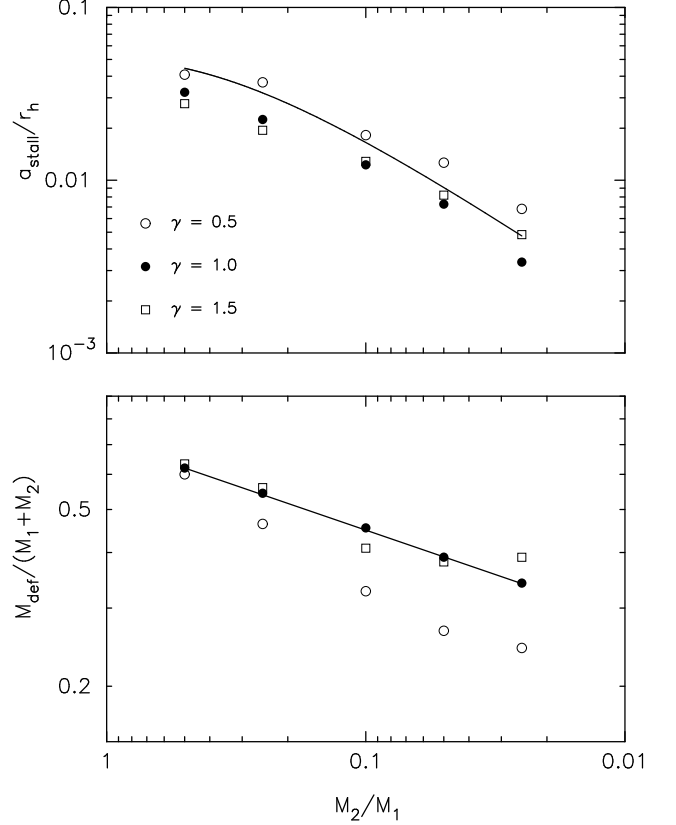

FIG. 4.— Stalling radius (a) and mass deficit at $t = t_{stall}$ (b) as functions of the binary mass ratio. Curve in (a) is Equation (12); curve in (b) is Equation (13).

ues. For instance, Figure 2 shows that the mass deficit in the $N = 200K$ integration of the $(\gamma = 1.0, q = 0.1)$ model varies only between $0.50 \lesssim M_{def}/M_1 \lesssim 0.65$ for $110 \leq t \leq 140$. Integrations with larger N will ultimately be required in order to improve on these estimates.

The results are presented in Table 1 and Figure 4. The upper panel of Figure 4 shows a_{stall} as a fraction of r'_h, the binary's influence radius (the radius containing a mass in stars equal to $M_1 + M_2$) at t_{stall}. The measured points are compared with

$$\frac{a_{stall}}{r'_h} = 0.2 \frac{q}{(1+q)^2}; \qquad (12)$$

this functional form was motivated by Equation (7). Given the likely uncertainties in the estimated a_{stall} values, Figure 4 suggests that there is no significant dependence of a_{stall}/r'_h on the initial nuclear density profile. This result will be used below to estimate stalling radii in observed galaxies.

The lower panel of Figure 4 shows mass deficits at $t = t_{stall}$ as a fraction of M_{12}. The line in this figure is

$$\frac{M_{def}}{M_{12}} = 0.70 q^{0.2}. \qquad (13)$$

This relation is a good fit to the $\gamma = 1.0$ and $\gamma = 1.5$ models, though it overestimates M_{def} for $\gamma = 0.5$. In any case, the dependence of M_{def} on binary mass ratio is weak, consistent with the prediction made above.

In galaxies with initially steep nuclear density profiles, $\rho \sim r^{-\gamma}$, $1.0 \lesssim \gamma \lesssim 1.5$, Figure 4 suggests that mass deficits generated by "stalled" binaries should lie in the narrow range

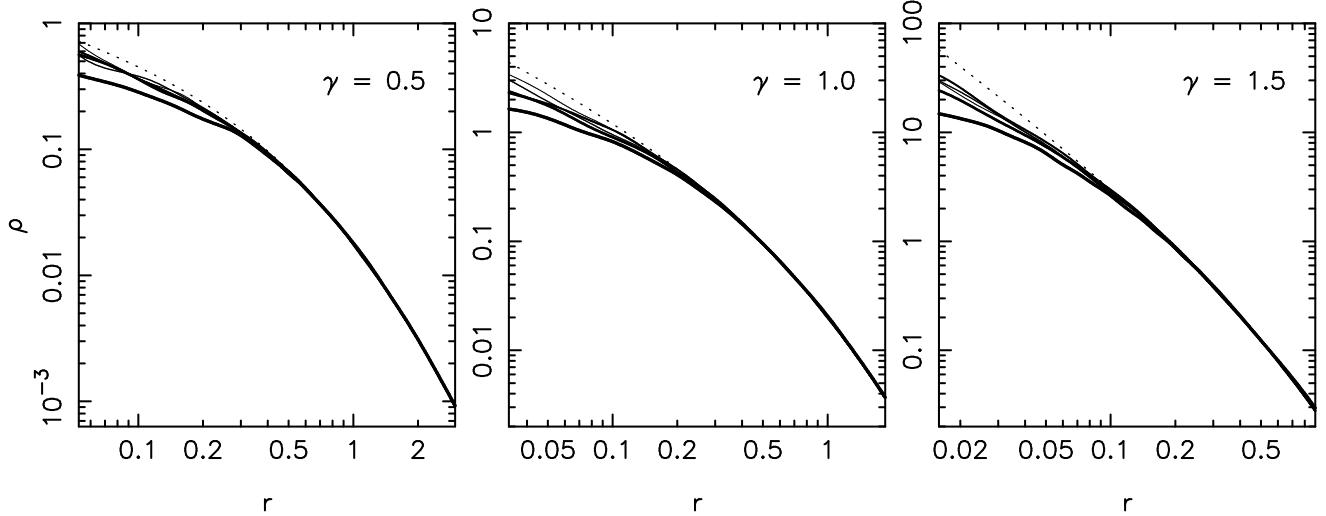$$0.4 \lesssim \frac{M_{def}}{M_1 + M_2} \lesssim 0.6, \quad 0.05 \lesssim q \lesssim 0.5. \qquad (14)$$

FIG. 5.— Density profiles at $t = t_{stall}$. Thickness of curves decreases from $q = 0.5$ to $q = 0.025$. Dotted lines are the initial density profiles.

To a good approximation, $M_{def} \approx 0.5M_\bullet$.

Density profiles at $t = t_{stall}$ are shown in Figure 5. It is interesting that none of the profiles exhibits the very flat, nearly constant density cores seen in some bright elliptical galaxies (Kormendy 1985; Lauer et al. 2002; Ferrarese et al. 2006).

5. MULTI-STAGE MERGERS

The weak dependence of M_{def}/M_{12} on initial density profile and on q found above has an obvious implication: in repeated mergers, mass deficits should increase cumulatively, even if expressed as a multiple of $M_\bullet$, the combined mass of the two SBHs at the end of each merger. If the stellar mass displaced in a single merger is $\sim 0.5M_{12}$, then (assuming that the two SBHs always coalesce before the next SBH falls in) the mass deficit following $\mathcal{N}$ mergers with $M_2 \ll M_1$ is $\sim 0.5\mathcal{N}M_\bullet$ with $M_\bullet$ the accumulated mass of the SBH.

Equation (13) could be used to derive a more precise prediction for the dependence of the mass deficit on $\mathcal{N}$. But direct simulation is a better approach. To this end, multi-stage N-body integrations were carried out. The starting point for each set of integrations was one of the $\gamma = 1.5$, $M_1 = 0.01$ N-body models described above, extracted at $t = t_{stall}$. The two massive particles were replaced by a single particle with mass equal to their combined mass, and with position and velocity equal to the center-of-mass values for the binary. A second massive particle, with mass equal to the original value of M_2, was then added and the model integrated forward until the new stalling radius was reached. The process was then repeated. In each set of experiments, the mass M_2 of the second SBH particle was kept fixed; in other words, $M_\bullet$, the accumulated central mass, increased linearly with the number $\mathcal{N}$ of mergers, while the binary mass ratio decreased with $\mathcal{N}$. Three different values of M_2 were tried: $M_2 = (0.005, 0.0025, 0.001)$.

Figure 6 and Table 2 give the results. The cumulative effect of multiple mergers is clear from the figure: $M_{def}/M_\bullet$ increases roughly linearly with $\mathcal{N}$ for the first few mergers, reaching values of ~ 1 for $\mathcal{N} = 2$ and ~ 1.5 for $\mathcal{N} = 3$. For larger $\mathcal{N}$ and for smaller M_2, the increase of $M_{def}/M_\bullet$ with $\mathcal{N}$ begins to drop below a linear relation. That this should be so is clear from the results of the single-stage mergers (Figure 4). Nevertheless, Figure 6 verifies that (at least for $q \gtrsim 0.1$) hierarchical mergers produce mass deficits that scale roughly

TABLE 2
MULTI-STAGE N-BODY INTEGRATIONS

M_2	$\mathcal{N}$	$M_\bullet$	M_{def}	$M_{def}/M_\bullet$	$M_{def}/(\mathcal{N}M_\bullet)$
0.0050	1	0.0150	0.0095	0.63	0.63
	2	0.0200	0.024	1.20	0.60
	3	0.0250	0.041	1.64	0.55
	4	0.0300	0.057	1.90	0.48
0.0025	1	0.0125	0.0070	0.56	0.56
	2	0.0150	0.017	1.13	0.57
	3	0.0175	0.027	1.54	0.51
	4	0.0200	0.035	1.75	0.44
0.0010	1	0.0110	0.004	0.41	0.41
	2	0.0120	0.010	0.79	0.40
	3	0.0130	0.014	1.10	0.37
	4	0.0140	0.018	1.29	0.32

linearly with both $\mathcal{N}$ and $M_\bullet$ for small $\mathcal{N}$.

Of course, these results are only meaningful under the assumption that the binary manages to coalesce between successive merger events. Infall of a SBH into a nucleus containing an uncoalesced binary would almost certainly result in *larger* values of $M_{def}/M_\bullet$ than those given in Table 2, for reasons discussed below.

6. COMPARISON WITH OBSERVED MASS DEFICITS

Mass deficits, computed from observed luminosity profiles, have been published for a number of "core" galaxies (Milosavljevic et al. 2002; Ravindranath, Ho & Filippenko 2002; Graham 2004; Ferrarese et al. 2006). As first emphasized by Milosavljevic et al. (2002), computing M_{def} is problematic due to the unknown form of the galaxy's luminosity profile before it was modified by the binary. Graham (2004) noted that Sersic's law provides the best global fit to the luminosity profiles of early-type galaxies and bulges and proposed that mass deficits be defined in terms of the deviation of the inner profile from the best-fitting Sersic law. This procedure was followed also by Ferrarese et al. (2006) in their study of Virgo galaxies using HST/ACS data.

Figure 7 summarizes the results from the Graham (2004) and Ferrarese et al. (2006) studies. Mass deficits from Graham (2004) were increased by 0.072 in the logarithm to correct an error in the mass-to-light ratios (A. Graham, private communication). Graham (2004) gives two estimates of $M_\bullet$ for each galaxy, based on the empirical correlation
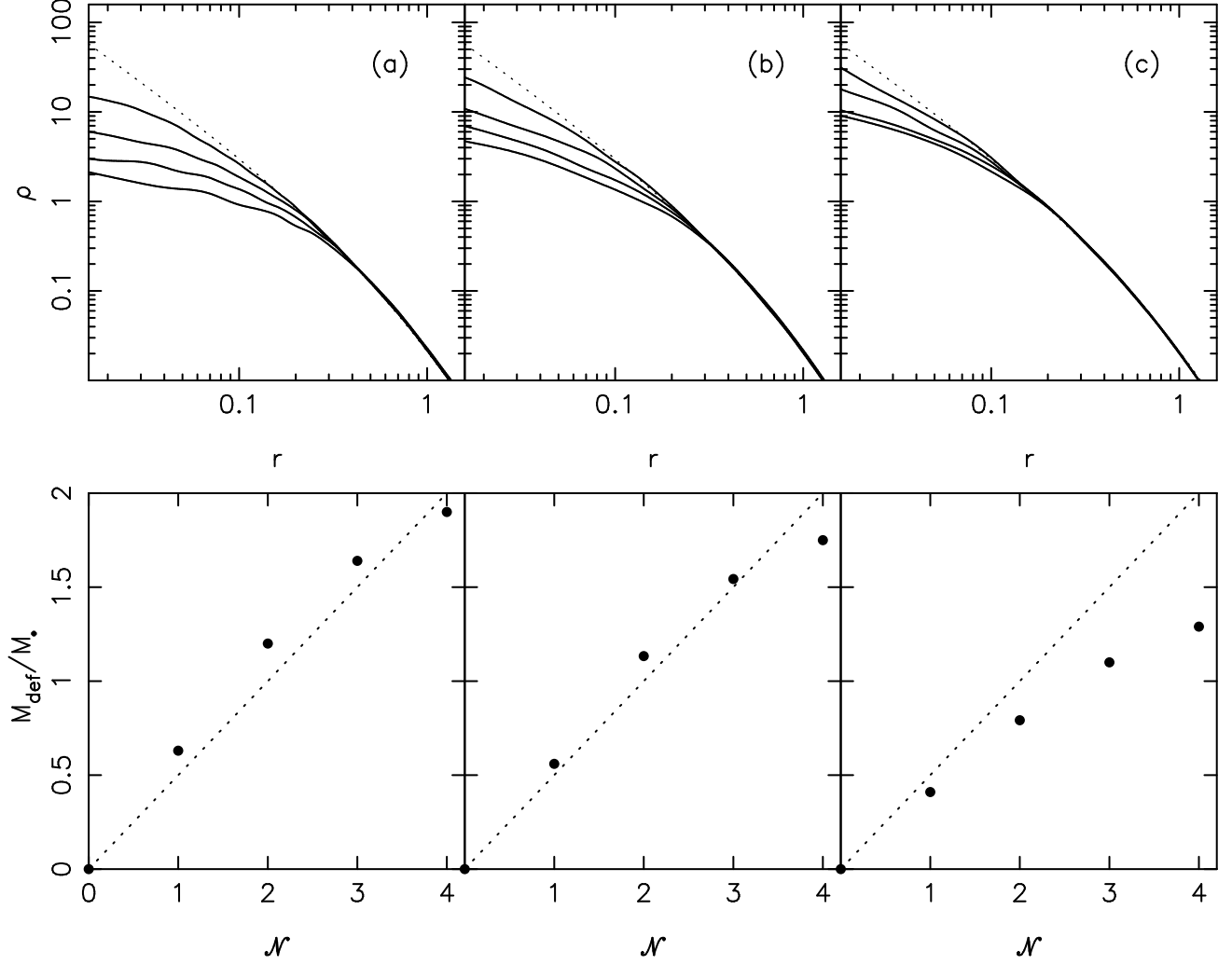
FIG. 6.— Density profiles and mass deficits in the multi-stage integrations. (a) $M_2 = 0.005$; (b) $M_2 = 0.0025$; (c) $M_2 = 0.001$. In the upper panels, dotted lines show the initial density profile and solid lines show $\rho(r)$ at the end of each merger, i.e. at $t = t_{stall}$. In the lower panels, points show $M_{def}/M_\bullet$ at t_{stall} and dotted lines show $M_{def}/M_\bullet = 0.5\mathcal{N}$, where $M_\bullet$ is the accumulated SBH mass.
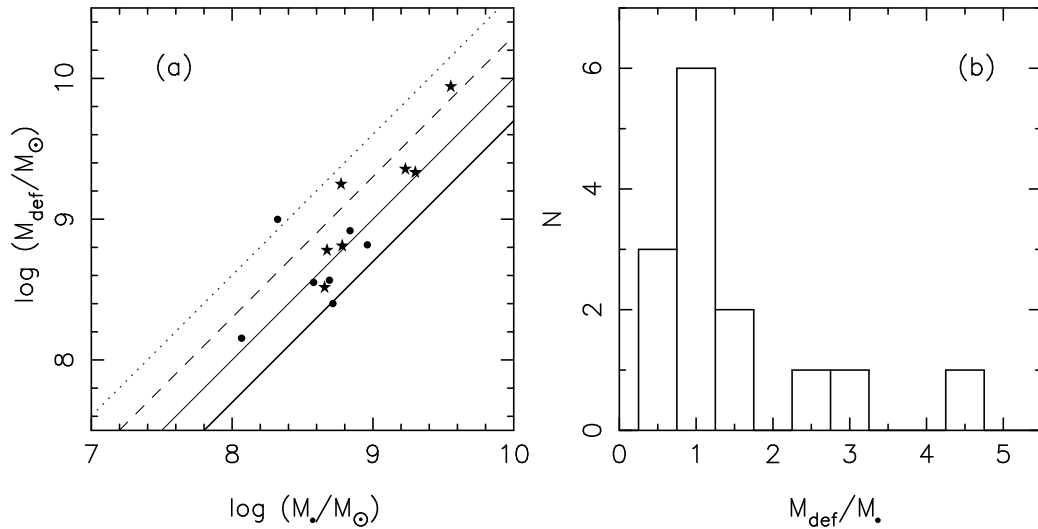
FIG. 7.— (a) Observed mass deficits from Graham (2004) (filled circles) and Ferrarese et al. (2006) (stars). Thick, thin, dashed and dotted lines show $M_{def}/M_\bullet = 0.5, 1, 2$ and 4 respectively. (b) Histogram of $M_{def}/M_\bullet$.

with concentration parameter (Graham et al. 2001) and on the Gebhardt et al. (2000) version of the $M_\bullet - \sigma$ relation. We recomputed SBH masses for Graham's galaxies using the most current version of the $M_\bullet - \sigma$ relation (Ferrarese & Ford 2005). Ferrarese et al. (2006) computed $M_\bullet$ for their sample galaxies in the same way; we have replaced $M_\bullet$ for three of their galaxies (NGC4486, NGC4374, NGC4649) with values derived from detailed kinematical modelling (Macchetto et al. 1997; Bower et al. 1998; Gebhardt et al. 2003). One "core" galaxy from Ferrarese et al. (2006) – NGC 798 – was excluded since it contains a large-scale stellar disk.

The histogram of $M_{def}/M_\bullet$ values is shown in Figure 7b. There is a clear peak at $M_{def}/M_\bullet \approx 1$.

Sersic's law – which describes the projected, or surface, luminosity density of early-type galaxies – implies a *space* density that varies as $j(r) \sim r^{-\gamma}$ at small radii, where $\gamma \approx (n-1)/n$ and n is the Sersic index. The galaxies plotted in Figure 7 have $n \gtrsim 5$, hence $0.8 \lesssim \gamma \lesssim 1.0$; in other words, the mass deficits for these galaxies were computed under the assumption that the pre-existing nuclear density was a power law with $\gamma \approx 1$. This is approximately the same inner dependence as in our $\gamma = 1$ Dehnen-model galaxies. While the cumulative N-body mass deficits shown in Figure 6 and Table 2 were based on initial models with $\gamma = 1.5$, Figure 4 suggests that the results would have been almost identical for $\gamma = 1$, at least during the first few stages of the merger hierarchy.

Comparing Figures 6 and 7, we therefore conclude that most "core" galaxies have experienced $1 \lesssim \mathcal{N} \lesssim 3$ mergers (i.e. $0.5 \lesssim M_{def}/M_\bullet \lesssim 1.5$), with $\mathcal{N} = 2$ the most common value.

A few galaxies in Figure 7 have significantly larger mass deficits; the most extreme object is NGC 5903 with $M_{def}/M_\bullet \approx 4.5$. Of course the uncertainties associated with the M_{def} and $M_\bullet$ values in Figure 7 may be large; the former due to uncertain M/L corrections, the latter due to various difficulties associated with SBH mass estimation (e.g. Maciejewski & Binney 2001; Valluri, Merritt & Emsellem 2004). In the case of NGC 5903, for which $M_\bullet$ was computed from the $M_\bullet - \sigma$ relation, we note that published velocity dispersions for this galaxy range from 192 km s^{-1} (Smith et al. 2000) to 245 km s^{-1} (Davies et al. 1987); the corresponding range in the inferred black hole mass is $1.36 \times 10^8 \lesssim M_\bullet/M_\odot \lesssim 4.45 \times 10^8$ and the range in $M_{def}/M_\bullet$ is $1.9 \lesssim M_{def}/M_\bullet \lesssim 6.2$. Even if σ were known precisely, there will always be a substantial uncertainty associated with any $M_\bullet$ value derived from an empirical scaling relation.

But assuming for the moment that the numbers plotted in Figure 7 are accurate, how might the galaxies with $M_{def}/M_\bullet > 2$ be explained? There are several possibilities. (a) These galaxies are the product of $\mathcal{N} \gtrsim 4$ mergers. Two of the largest $M_{def}/M_\bullet$ values in Figure 7 are associated with M87 and M49, both extremely luminous galaxies that could have experienced multiple mergers. However, Figure 6 suggests that $M_{def}/M_\bullet$ values $\gtrsim 3$ might be difficult to produce via repeated mergers. (b) The primordial density profiles in these galaxies were flatter than Sersic's law at small radii. (c) The two SBHs failed to efficiently coalesce during one or more of the merger events, so that a binary was present when a third SBH fell in. Indeed this is likely to be the case in the largest (lowest density) galaxies in Figure 7, which have little gas and extremely long timescales for loss-cone repopulation by two-body relaxation. Infall of a third SBH onto an uncoalesced binary is conducive to smaller values of $M_\bullet$, since one

or more of the SBHs could eventually be ejected by the gravitational slingshot (Mikkola & Valtonen 1990); and to larger values of M_{def}, since multiple SBHs are more efficient than a binary at displacing stars (Merritt et al. 2004b). (The former point is only relevant to galaxies – unlike NGC 5903 – for which $M_\bullet$ has actually been measured.) The chaotic interaction between three SBHs would probably also assist in the gravitational wave coalescence of the two most massive holes by inducing random changes in their relative orbit (Blaes et al. 2002). (d) The gravitational-wave rocket effect is believed capable of delivering kicks to a coalescing binary as large as ~ 200 km s^{-1} (Favata et al. 2004; Blanchet et al. 2005; Herrmann et al. 2006; Baker et al. 2006). The stellar density drops impulsively when the SBH is kicked out, and again when its orbit decays via dynamical friction. Mass deficits produced in this way can be as large as $\sim M_\bullet$ (Merritt et al. 2004a; Boylan-Kolchin et al. 2004). (e) Stars bound to the infalling SBH – which were neglected in the N-body simulations presented here – might affect M_{def}, although it is not clear what the direction or magnitude of the change would be.

Focussing again on the majority of galaxies in Figure 7 with $0.5 \lesssim M_{def}/M_\bullet \lesssim 1.5$, we can ask whether values of $\mathcal{N}$ in the range $1 \leq \mathcal{N} \leq 3$ are consistent with hierarchical models of galaxy formation. If the seeds of the current SBHs were present at large redshift, the ancestry of a bright galaxy could include dozens of mergers involving binary SBHs (Volonteri et al. 2003a; Sesana et al. 2004). However the more relevant quantity is probably the number of mergers since the era at which most of the gas was depleted, since star formation from ambient gas could regenerate a density cusp after its destruction by a binary SBH (Graham 2004). Haehnelt & Kauffmann (2002) calculate just this quantity, based on semi-analytic models for galaxy mergers that include prescriptions for star- and SBH-formation. Their Figure 2 shows probability distributions for $\mathcal{N}$ as a function of galaxy luminosity for mergers with $q > 0.3$. For galaxies like those in Figure 7 ($M_V \lesssim -21, M_B \lesssim -20$), Haehnelt & Kauffmann (2002) find a median $\mathcal{N}$ of ~ 1, but particularly among the brightest galaxies, they find that values of $\mathcal{N}$ as large as 3 or 4 are also likely. This prediction is consistent with Figure 7.

Probably the biggest uncertainty in this analysis is the unknown behavior of the binary after it reaches $a \approx a_{stall}$ and before the next SBH falls in. If mergers are "dry," gas-dynamical torques can not be invoked to accelerate the coalescence, implying a complicated interaction between three SBHs when the next merger event occurs. As discussed above, the net effect would be an increase in $M_{def}/M_\bullet$. On the other hand, if gas *is* present in sufficient quantities to assist in coalescence, it may also form new stars – decreasing M_{def} – and/or accrete onto the SBH – increasing $M_\bullet$; in either case, $M_{def}/M_\bullet$ would be smaller than computed here.

7. STALLED BINARY SEPARATIONS

Equation (12) gives an estimate for the stalling radius of a binary SBH in terms of its influence radius r_h'; the latter is defined as the radius of a sphere containing a stellar mass equal to twice $M_\bullet \equiv M_1 + M_2$, *after* the binary has reached a_{stall}, i.e. after it has finished modifying the stellar density profile. One can use Equation (12) to estimate binary separations in galaxies where $M_\bullet$ and $\rho(r)$ are known, under the assumption (discussed in more detail below) that no additional mechanism has induced the binary to evolve beyond a_{stall}. Table 3 gives the results for the seven Virgo "core" galax-

Galaxy (1)	B_T (2)	$M_\bullet$ (3)	r'_h (4)	a_{stall} $q = 0.5$ (5)	a_{stall} $q = 0.1$ (6)	v_{ej} (7)	v_{esc} (8)	v_{esc} (9)
NGC 4472	-21.8	5.94	130. (1.6)	5.6 (0.070)	2.1 (0.026)	562.	1395	1865
NGC 4486	-21.5	35.7	460. (5.7)	20. (0.25)	7.6 (0.095)	733.	1480	2175
NGC 4649	-21.3	20.0	230. (2.9)	10. (0.13)	3.8 (0.047)	776.	1596	2272
NGC 4406	-21.0	4.54	90. (1.1)	4.0 (0.050)	1.5 (0.019)	590.	1253	1790
NGC 4374	-20.8	17.0	170. (2.1)	7.6 (0.094)	2.8 (0.035)	832.	1605	1865
NGC 4365	-20.6	4.72	115. (1.4)	5.0 (0.063)	1.9 (0.023)	533.	1145	1615
NGC 4552	-20.3	6.05	73. (0.91)	3.2 (0.040)	1.2 (0.015)	757.	1500	2230

Notes. – Col. (1): New General Catalog (NGC) numbers. Col. (2): Absolute B-band galaxy magnitudes. Col. (3): Black hole masses in $10^8 M_\odot$. Col. (4): Black hole influence radii, defined as the radii containing a mass in stars equal to $2M_\bullet$, in pc (arcsec). Col. (5): Binary stalling radii for $q = 0.5$, in pc (arcsec). Col. (6): Binary stalling radii for $q = 0.1$, in pc (arcsec). Col. (7): Typical ejection velocity from a binary SBH with $a = a_{stall}$ (km s^{-1}). Cols. (8), (9): Escape velocity (km s^{-1}).

ies shown in Figure 7. Influence radii were computed using parametric ("core-Sersic") fits to the luminosity profiles, as described in Ferrarese et al. (2006); that paper also gives the algorithm which was used for converting luminosity densities into mass densities. When discussing real galaxies, r'_h is just the currently-observed influence radius r_h and henceforth the prime is dropped.

Stalling radii are given in Table 3 assuming $q = 0.5$ and $q = 0.1$; a_{stall} for other values of q can be computed from Equation (12). Table 3 also gives angular sizes of the binaries assuming a distance to Virgo of 16.52 Mpc. Typical separations between components in a stalled binary are found to be ~ 10 pc ($0.1''$) ($q = 0.5$) and ~ 3 pc ($0.03''$) ($q = 0.1$). Of course these numbers should be interpreted as upper limits; nevertheless they are large enough to suggest that binary SBHs might be resolvable in the brighter Virgo galaxies if both SBHs are luminous.

8. DISCUSSION

We have shown that the mass deficit produced by a binary SBH at the center of a spherical galaxy is "quantized" in units of $\sim 0.5(M_1 + M_2)$, with only a weak dependence on binary mass ratio, and that $M_{def}/M_\bullet$ grows approximately linearly with the number of merger events. These results were compared with observed mass deficits to conclude that most bright elliptical galaxies have experienced $1 - 3$ mergers since the era at which gas was depleted and/or star formation became inefficient.

In this section, we explore some further implications of the N-body results, and discuss their generality.

8.1. *Loss-Cone Refilling and Non-Spherical Geometries*

The approach adopted in this paper was motivated by the fact that mass deficits, or cores, are only observed at the centers of galaxies with very long relaxation times. In such galaxies, collisional repopulation of orbits depleted by the binary would act too slowly to significantly influence the binary's evolution (Valtonen 1996), and the binary would stop evolving once it had interacted with all stars on intersecting orbits. But even in the completely collisionless case, evolution of the binary, and its effect on the local distribution of stars, could be different in nonspherical (axisymmetric, triaxial, ...) geometries. There are really two questions here: (a) How does

a_{stall} depend on geometry? (b) If a binary continues to harden below a_{stall}, what would be the effect on M_{def}?

The answer to the latter question is complex. Consider a galaxy containing a stalled binary, and suppose that some mechanism – gravitational encounters, time-dependent torques from a passing galaxy, perturbations from a third SBH, new star formation, etc. – has the net effect of placing additional stars on orbits that intersect the binary. These stars will be ejected, and the binary will shrink. However there need not be any net change in the mass deficit, since the new stars are first added, then subtracted, from the nuclear density. (Second-order changes in ρ due to the time dependence of the gravitational potential are being ignored.) This argument suggests that the good correlation found here (Figure 4) between a_{stall} and M_{def} need not apply more generally, in time-dependent or non-spherical situations.

An example of the latter is a binary embedded in a triaxial galaxy which contains centrophilic (box or chaotic) orbits. The mass in stars on centrophilic orbits can be extremely large, $\gg M_\bullet$, in a triaxial galaxy, although many orbital periods will generally be required before any given star passes near enough to the binary to interact with it (Merritt & Poon 2004; Holley-Bockelmann & Sigurdsson 2006). Nevertheless the binary need not stall (Berczik et al. 2006). Self-consistent calculations of the effect of a binary on the nuclear density profile have not been carried out in the triaxial geometry, but it is clear that mass deficits might be smaller than in the spherical geometry since some stars ejected by the binary will be on orbits with very large ($\gg r_h$) characteristic radii.

The influence of different geometries on a_{stall} and M_{def} will be investigated in future papers.

8.2. *Mass Deficits and Core Radio Power*

An intriguing relation was discovered by Balmaverde & Capetti (2006) and Capetti & Balmaverde (2006) between the radio and morphological properties of active galaxies. Radio-loud AGN – active nuclei with a large ratio of radio to optical or radio to X-ray luminosities – are *uniquely* associated with "core" galaxies. In fact, the slope of the inner brightness profile appears to be the *only* quantity that reliably predicts whether an AGN is radio-loud or radio-quiet. Capetti & Balmaverde (2006) also showed that when the radio-loud and radio-quiet galaxies are considered separately, there is no dependence of radio loudness on the nuclear density profile within either class. In other words, the fact that an active galaxy is morphologically a "core" galaxy predicts that it will be radio-loud but does not predict how loud. While the origin of this connection is unclear, it might reflect the influence of SBH rotation on radio power (Wilson & Colbert 1995): "core" galaxies have experienced a recent merger, and coalescence of the two SBHs resulted in a rapidly-spinning remnant.

Two results from the N-body work presented here may be relevant to the Capetti & Balmaverde correlation. First, as shown above, the mass deficit is a weak function of the mass ratio of the binary that produced it, i.e., the shape of the nuclear density profile is poorly correlated with the mass of the infalling hole. Since the degree of spin-up is also weakly correlated with M_2/M_1 (Wilson & Colbert 1995; Merritt & Ekers 2002; Hughes & Blandford 2003) – even very small infalling holes can spin up the larger hole to near-maximal spins – it follows that SBH rotation should be poorly correlated with mass deficit. This may explain the weak dependence of radio loudness on profile slope found by

Capetti & Balmaverde (2006) for the core galaxies.

Second, as argued above, core galaxies may contain uncoalesced binaries. Perhaps the presence of a second SBH is the main factor that determines radio loudness.

8.3. *High-Velocity Stars*

Gravitational slingshot ejections by a binary SBH produce a population of high-velocity stars with trajectories directed away from the center of the galaxy. A few hyper-velocity stars have been detected in the halo of the Milky Way (Brown et al. 2005; Hirsch et al. 2005; Brown et al. 2006), and a binary SBH at the Galactic center is a possible model for their origin. The short nuclear relaxation time would accelerate the hardening of a massive binary by ensuring that stars were scattered into its sphere of influence (Yu & Tremaine 2003). In this model, stars could have been ejected during the late stages of the binary's evolution, when $a \ll a_h$, at high enough velocities and large enough numbers to explain the observed hyper-velocity stars.

Binary SBHs have also been invoked to explain other populations, e.g. intergalactic planetary nebulae in the Virgo cluster (Arnaboldi et al. 2004). If every Virgo galaxy harbored a binary SBH with mass ratio $q = 0.1$ which evolved, via slingshot ejection of stars, to the gravitational-radiation regime, the total mass ejected would have been $\sim 2\%$ of the luminous mass of the cluster (Holley-Bockelmann et al. 2005). But at least in the brighter Virgo galaxies – including the galaxies in Table 3 – two-body relaxation times are much too long for collisional resupply of binary loss cones, and there is no compelling reason to assume that the binary SBHs in these galaxies would have continued interacting with stars beyond a_{stall}. At these separations, velocities between the two components of the binary are relatively modest, implying a much lower probability of ejection of stars at velocities large enough to escape the galaxy.

The mean specific energy change of a star that interacts with a hard binary is $\sim 3G\mu/2a$ (Hills 1983; Quinlan 1996). Combining this with Equation (12) for a_{stall} gives the typical ejection velocity from a stalled binary:

$$v_{ej} \approx 4.0 \left(\frac{GM_{12}}{r_h} \right)^{1/2} \approx 830\,\mathrm{kms}^{-1} \left(\frac{M_{12}}{10^8 M_\odot} \right)^{1/2} \left(\frac{r_h}{10\,\mathrm{pc}} \right)^{-1/2} , \quad (15)$$

independent of mass ratio. Of course this is an upper limit in the sense that ejection velocities are lower when $t < t_{stall}$. Table 3 gives v_{ej} for the Virgo "core" galaxies and also v_{esc}, the escape velocity, defined as $\sqrt{-2\Phi(a_{stall})}$ with $\Phi(r)$ the gravitational potential including the contribution from the binary, modelled as a point with mass equal to the currently-observed value of $M_\bullet$. Ejection velocities are seen to be much smaller than v_{esc} in all cases, implying that essentially no stars would be ejected into the intracluster medium.

8.4. *Dark-Matter Cores*

The specific energy change of a dark matter particle interacting with a binary SBH is identical to that of a star. At least in the case of bright elliptical galaxies like those in Table 3, it is unlikely that dark matter was ever a dominant component near the center or that it significantly influenced the evolution of the binary. But ejection of dark matter particles by a massive binary would produce a core in the dark matter distribution similar in size to the luminous-matter core, $r_{core} \approx r_h$. A more definite statement about the variation with radius of $\rho_{DM}/\rho_\star$ near the center of a galaxy containing a binary SBH is probably impossible to make without N-body simulations that contain all three components. However Table 3 suggests dark matter core radii of hundreds of parsecs in bright elliptical galaxies.

It follows that the rates of self-interaction of supersymmetric particles at the centers of galaxies like M87 (Baltz et al. 2000) would be much lower than computed under the assumption that the dark matter still retains its "primordial" density profile (Navarro et al. 1996; Moore et al. 1998). This fact has implications for so-called "indirect" dark matter searches, in which inferences are drawn about the properties of particle dark matter based on measurements of its self-annihilation byproducts (Bertone et al. 2004). One of the proposed search strategies is to identify a component of the diffuse gamma-ray background that is generated by dark matter annihilations in halos at all redshifts (Ullio et al. 2002; Taylor & Silk 2003). Calculations of the background flux (Ando 2005; Elsässer & Mannheim 2005) have so far always assumed that the dark matter distribution does not change with time. Since the annihilation flux in a smooth dark matter halo is dominated by the the center, these calculations may substantially over-estimate the contribution of galactic halos to the gamma-ray background.

REFERENCES

Aarseth, S. J. 1999, PASP, 111, 1333
Alexander, T. 1999, ApJ, 527, 835
Ando, S. 2005, Physical Review Letters, 94, 171303
Arnaboldi, M., Gerhard, O., Aguerri, J. A. L., Freeman, K. C., Napolitano, N. R., Okamura, S., & Yasuda, N. 2004, ApJ, 614, L33
Bahcall, J. N. & Wolf, R. A. 1976, ApJ, 209, 214
Baker, J. G., Centrella, J., Choi, D.-I., Koppitz, M., van Meter, J. R., & Miller, M. C. 2006, arXiv:astro-ph/0603204
Balmaverde, B., & Capetti, A. 2006, A&A, 447, 97
Baltz, E. A., Briot, C., Salati, P., Taillet, R., & Silk, J. 2000, Phys. Rev. D, 61, 023514
Baumgardt, H., Makino, J., & Ebisuzaki, T. 2004, ApJ, 613, 1133
Baumgardt, H., Makino, J., & Ebisuzaki, T. 2004, ApJ, 613, 1143
Begelman, M. C., Blandford, R. D. & Rees, M. J. 1980, Nature, 287, 307
Berczik, P., Merritt, D. & Spurzem, R. 2005, astro-ph/0507260
Berczik, P., Merritt, D., Spurzem, R., & Bischof, H.-P. 2006, ArXiv Astrophysics e-prints, arXiv:astro-ph/0601698
Bertone, G., Hooper, D., & Silk, J. 2004, Phys. Rep., 405, 279
Bertone, G., & Merritt, D. 2005, Modern Physics Letters A, 20, 1021
Blaes, O., Lee, M. H., & Socrates, A. 2002, ApJ, 578, 775
Blanchet, L., Qusailah, M. S. S., & Will, C. M. 2005, ApJ, 635, 508
Bower, G. A., et al. 1998, ApJ, 492, L111
Boylan-Kolchin, M., Ma, C.-P., & Quataert, E. 2004, ApJ, 613, L37
Brown, W. R., Geller, M. J., Kenyon, S. J., & Kurtz, M. J. 2005, ApJ, 622, L33
Brown, W. R., Geller, M. J., Kenyon, S. J., & Kurtz, M. J. 2006, ArXiv Astrophysics e-prints, arXiv:astro-ph/0601580
Capetti, A. & Balmaverde, B. 2006, ArXiv Astrophysics e-prints, arXiv:astro-ph/0603345
Chandrasekhar, S. 1943, ApJ, 97, 255

Chatterjee, P., Hernquist, L., & Loeb, A. 2003, ApJ, 592, 32

Clutton-Brock, M. 1973, Ap&SS, 23, 55

Davies, R. L., Burstein, D., Dressler, A., Faber, S. M., Lynden-Bell, D., Terlevich, R. J., & Wegner, G. 1987, ApJS, 64, 581

Dehnen, W. 1993, MNRAS, 265, 250

Dorband, E. N., Hemsendorf, M., & Merritt, D. 2003, Journal of Computational Physics, 185, 484

Elsässer, D., & Mannheim, K. 2005, Physical Review Letters, 94, 171302

Faber, S. M. et al. 1997, AJ, 114, 1771

Favata, M., Hughes, S. A., & Holz, D. E. 2004, ApJ, 607, L5

Ferrarese, L., et al. 2006, ArXiv Astrophysics e-prints, arXiv:astro-ph/0602297

Ferrarese, L., & Ford, H. 2005, Space Science Reviews, 116, 523

Ferrarese, L., & Merritt, D. 2000, ApJ, 539, L9

Fukushige, T., Makino, J., & Kawai, A. 2005, PASJ, 57, 1009

Gebhardt, K. et al. 1996, AJ, 112, 105

Gebhardt, K., et al. 2000, ApJ, 539, L13

Gebhardt, K., et al. 2003, ApJ, 583, 92

Genzel, R., Schödel, R., Ott, T., Eisenhauer, F., Hofmann, R., Lehnert, M., Eckart, A., Alexander, T., Sternberg, A., Lenzen, R., ClÃ©net, Y., Lacombe, F., Rouan, D., Renzini, A., & Tacconi-Garman, L. E. ApJ, 594, 812

Gopal-Krishna, Biermann, P. L., & Wiita, P. J. 2003, ApJ, 594, L103

Graham, A. W., Erwin, P., Caon, N., & Trujillo, I. 2001, ApJ, 563, L11

Graham, A. W. 2004, ApJ, 613, L33

Graham, A. W., & Guzmán, R. 2003, AJ, 125, 2936

Gualandris, A., Portegies Zwart, S., & Tirado-Ramos, A. 2004, ArXiv Astrophysics e-prints, arXiv:astro-ph/0412206

Haardt, F., Sesana, A., & Madau, P. 2006, ArXiv Astrophysics e-prints, arXiv:astro-ph/0601705

Haehnelt, M. G., & Kauffmann, G. 2002, MNRAS, 336, L61

Hemsendorf, M., Sigurdsson, S., & Spurzem, R. 2002, ApJ, 581, 1256

Hernquist, L., & Ostriker, J. P. 1992, ApJ, 386, 375

Herrmann, F., Shoemaker, D., & Laguna, P. 2006, ArXiv General Relativity and Quantum Cosmology e-prints, arXiv:gr-qc/0601026

Hills, J. G. 1983, AJ, 88, 1269

Hirsch, H. A., Heber, U., O'Toole, S. J., & Bresolin, F. 2005, A&A, 444, L61

Holley-Bockelmann, K., Sigurdsson, S., Mihos, J. C., Feldmeier, J. J., Ciardullo, R., & McBride, C. 2005, ArXiv Astrophysics e-prints, arXiv:astro-ph/0512344

Holley-Bockelmann, K., & Sigurdsson, S. 2006, ArXiv Astrophysics e-prints, arXiv:astro-ph/0601520

Hooper, D., de la Calle Perez, I., Silk, J., Ferrer, F., & Sarkar, S. 2004, Journal of Cosmology and Astro-Particle Physics, 9, 2

Hughes, S. A., & Blandford, R. D. 2003, ApJ, 585, L101

Iwasawa, M., Funato, Y., & Makino, J. 2005, ArXiv Astrophysics e-prints, arXiv:astro-ph/0511391

Komossa, S. 2003, AIP Conf. Proc. 686: The Astrophysics of Gravitational Wave Sources, 686, 161

Kormendy, J. 1985, ApJ, 292, L9

Lauer, T. et al. 1998, AJ, 116, 2263

Lauer, T. R., et al. 2002, AJ, 124, 1975

Macchetto, F., Marconi, A., Axon, D. J., Capetti, A., Sparks, W., & Crane, P. 1997, ApJ, 489, 579

Maciejewski, W., & Binney, J. 2001, MNRAS, 323, 831

Makino, J., & Funato, Y. 2004, ApJ, 602, 93

Merritt, D., & Ekers, R. D. 2002, Science, 297, 1310

Merritt, D., Mikkola, S. & Szell, A. 2005, in preparation

Merritt, D., Milosavljevic, M., Favata, M., Hughes, S. A. & Holz, D.E. 2004a, ApJ, 607, L9

Merritt, D., Milosavljevic, M., Verde, L. & Jimenez, R. 2002, Phys. Rev. Lett., 88, 191301

Merritt, D., Piatek, S., Portegies Zwart, S., & Hemsendorf, M. 2004b, ApJ, 608, L25

Merritt, D., & Poon, M. Y. 2004, ApJ, 606, 788

Merritt, D. & Szell, A. 2005, astro-ph/0510498

Merritt, D. & Wang, J. 2005, ApJ, 621, L101

Mikkola, S., & Aarseth, S. J. 1990, Celestial Mechanics and Dynamical Astronomy, 47, 375

Mikkola, S., & Aarseth, S. J. 1993, Celestial Mechanics and Dynamical Astronomy, 57, 439

Mikkola, S., & Valtonen, M. J. 1990, ApJ, 348, 412

Mikkola, S., & Valtonen, M. J. 1992, MNRAS, 259, 115

Milosavljevic, M. & Merritt, D. 2001, ApJ, 563, 34

Milosavljevic, M. & Merritt, D. 2003, ApJ, 596, 860

Milosavljevic, M., Merritt, D., Rest, A., & van den Bosch, F. C. 2002, MNRAS, 331, 51

Moore, B., Governato, F., Quinn, T., Stadel, J., & Lake, G. 1998, ApJ, 499, L5

Muñoz, J. A., Kochanek, C. S., & Keeton, C. R. 2001, ApJ, 558, 657

Navarro, J. F., Frenk, C. S., & White, S. D. M. 1996, ApJ, 462, 563

Quinlan, G. D. 1996, New Astron. 1, 35

Quinlan, G. D. 1997, New Astron. 2, 533

Ravindranath, S., Ho, L. C. & Filippenko, A. V. 2002, ApJ, 566, 801

Rest, A. et al. 2001, AJ, 121, 2431

Romero, G. E., Chajet, L., Abraham, Z., & Fan, J. H. 2000, A&A, 360, 57

Roos, N., Kaastra, J. S., & Hummel, C. A. 1993, ApJ, 409, 130

Sesana, A., Haardt, F., Madau, P., & Volonteri, M. 2004, ApJ, 611, 623

Smith, R. J., Lucey, J. R., Hudson, M. J., Schlegel, D. J., & Davies, R. L. 2000, MNRAS, 313, 469

Spinnato, P. F., Fellhauer, M., & Portegies Zwart, S. F. 2003, MNRAS, 344, 22

Spitzer, L. 1987, "Dynamical Evolution of Globular Clusters" (Princeton: Princeton University Press)

Taylor, J. E., & Silk, J. 2003, MNRAS, 339, 505

Tremaine, S. et al. 1994, AJ, 107, 634

Ullio, P., Bergström, L., Edsjö, J., & Lacey, C. 2002, Phys. Rev. D, 66, 123502

Valluri, M., Merritt, D., & Emsellem, E. 2004, ApJ, 602, 66

Valtaoja, E., Teräsranta, H., Tornikoski, M., Sillanpää, A., Aller, M. F., Aller, H. D., & Hughes, P. A. 2000, ApJ, 531, 744

Valtonen, M. J. 1996, Comments on Astrophysics, 18, 191

van Albada, T. S., & van Gorkom, J. H. 1977, A&A, 54, 121

Volonteri, M., Haardt, F., & Madau, P. 2003, ApJ, 582, 559

Volonteri, M., Madau, P., & Haardt, F. 2003, ApJ, 593, 661

Wang, J. & Merritt, D. 2004, ApJ, 600, 149

Wilson, A. S., & Colbert, E. J. M. 1995, ApJ, 438, 62

Xie, G.-Z. 2003, Publications of the Yunnan Observatory, 95, 107

Yu, Q. 2002, MNRAS, 331, 935

Yu, Q., & Tremaine, S. 2003, ApJ, 599, 1129

Zier, C., & Biermann, P. L. 2001, A&A, 377, 23